RESEARCH ARTICLE

Key Points:
- Southern Greenland precipitation is largely driven by topography and wind direction
- Recent enhanced increase of Arctic temperature linked with increase of southwest Greenland precipitation
- Positive feedback mechanisms in Arctic amplification linked with increase in southwest Greenland precipitation

Examination of precipitation variability in southern Greenland

Jeffrey D. Auger[1] , Sean D. Birkel[1,2] , Kirk A. Maasch[1,2], Paul A. Mayewski[1,2] , and Keah C. Schuenemann[3]

[1]Climate Change Institute, University of Maine, Orono, Maine, USA, [2]School of Earth and Climate Sciences, University of Maine, Orono, Maine, USA, [3]Department of Earth and Atmospheric Sciences, Metropolitan State University of Denver, Denver, Colorado, USA

Abstract The surface mass balance of the Greenland ice sheet has decreased in recent decades with important implications for global sea level rise. Here a climate reanalysis model is used to examine observed circulation variability and changes in precipitation across southern Greenland to gain insight into the future climate in the region. The influence on precipitation from the North Atlantic Oscillation (NAO), Atlantic Multidecadal Oscillation (AMO), Icelandic Low, Azores High, regional blocking patterns, and near-surface temperature and winds are explored. Statistically significant correlations are higher between precipitation and the Icelandic Low and near-surface winds (0.5–0.7; $p < 0.05$) than correlations between precipitation and either the NAO or AMO climate indices (southwest Greenland: $r = 0.12$ and 0.28, respectively; and southeast Greenland: $r = 0.25$ and -0.07, respectively). Moreover, the recent enhanced warming in the Arctic (Arctic amplification) and the increase in the Greenland Blocking Index coincide with increased mean annual precipitation and interannual variability in southwest Greenland.

1. Introduction

The Greenland ice sheet contains the equivalent of ~6.7 m of global sea level and constitutes a laterally extensive, high albedo surface that impacts the Northern Hemisphere radiation balance by reflecting ~70% of the local incoming solar radiation [*Ohmura and Reeh*, 1991; *Tedesco et al.*, 2015]. By identifying atmospheric teleconnections that modulate moisture and heat transport to the ice sheet, future climate projections of mass balance can be improved.

This study utilizes the Japanese Meteorological Agency 55 Year Reanalysis [JRA-55; *Kobayashi et al.*, 2015] model to evaluate dominant atmospheric circulation patterns that control precipitation delivery to southern Greenland and therefore have an impact on the overall mass balance of the ice sheet and future sea level rise. First, the climate of Greenland is presented, and then the interannual variability of precipitation in southwest and southeast Greenland is discussed. We focus the study on meteorological variables that influence ice sheet mass balance: near-surface temperature, mean sea level pressure, and near-surface wind, with a particular focus on precipitation. As these variables are closely related to climate oscillations in the North Atlantic, we consider linkages between temperature, wind, and precipitation and local climate indices, including the North Atlantic Oscillation (NAO) and Atlantic Multidecadal Oscillation (AMO).

1.1. Southern Greenland and North Atlantic Climate

Our examination of the atmospheric patterns linked with southern Greenland precipitation involves a survey of diagnostic meteorological metrics. Two meter air temperature (T_{2m}, Figure 1a), mean sea level pressure (MSLP, Figure 1b), 10 m zonal (u) and meridional (v) winds (u_{10m}, Figure 1c; and v_{10m}, Figure 1d), and liquid water equivalent precipitation (Figure 1e) in southern Greenland are heavily impacted by the topographic divide of the ice sheet, a ridge along the 44°W longitude; this meridian has been used as a dividing line here between southeast and southwest. The high-altitude surface of the Greenland ice sheet induces strong anticyclonic katabatic winds, most prominent during winter months, known as the Greenland High (orange center in Figure 1b), and serves as a topographic barrier that facilitates large hydraulic jumps and the formation of lee-side troughs over the Denmark Strait [*Doyle et al.*, 2005]. The longitudinal ridge is prominent enough to create two major climate regimes. Temperature is coldest along the ridge and increases toward the coastline, with a shallower T_{2m} gradient to the west and a steeper gradient to the east. Flow across southwest Greenland is dominated by comparatively dry southeasterly winds, whereas flow across the southeast is
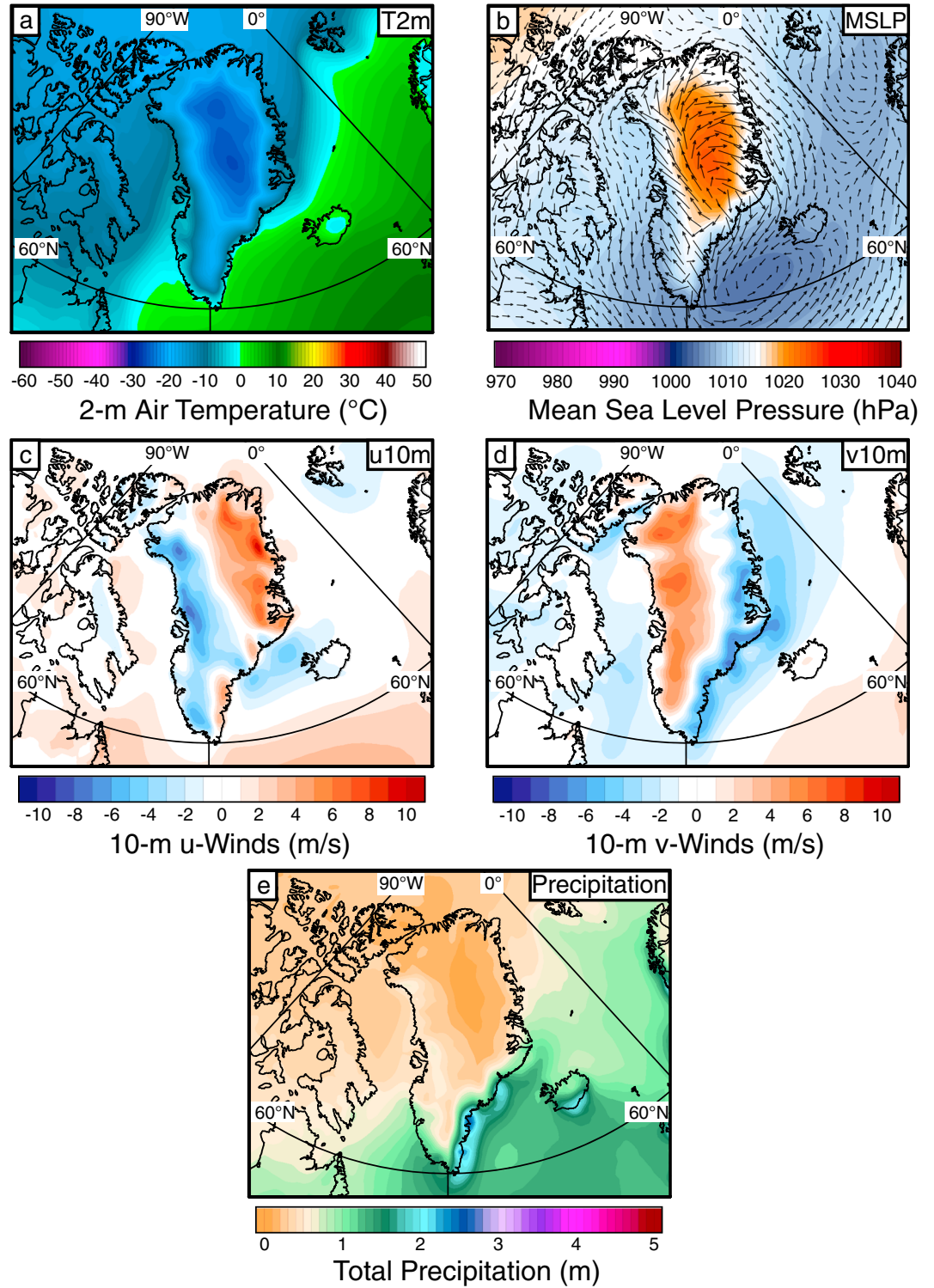
Figure 1. Greenland annual climatology showing (a) 2 m air temperature (T_{2m}), (b) mean sea level pressure (MSLP; shading) with 10 m horizontal winds (vectors), (c) 10 m u winds (u_{10m}), (d) 10 m v winds (v_{10m}), and (e) precipitation averaged over the JRA-55 record, 1958–2013.
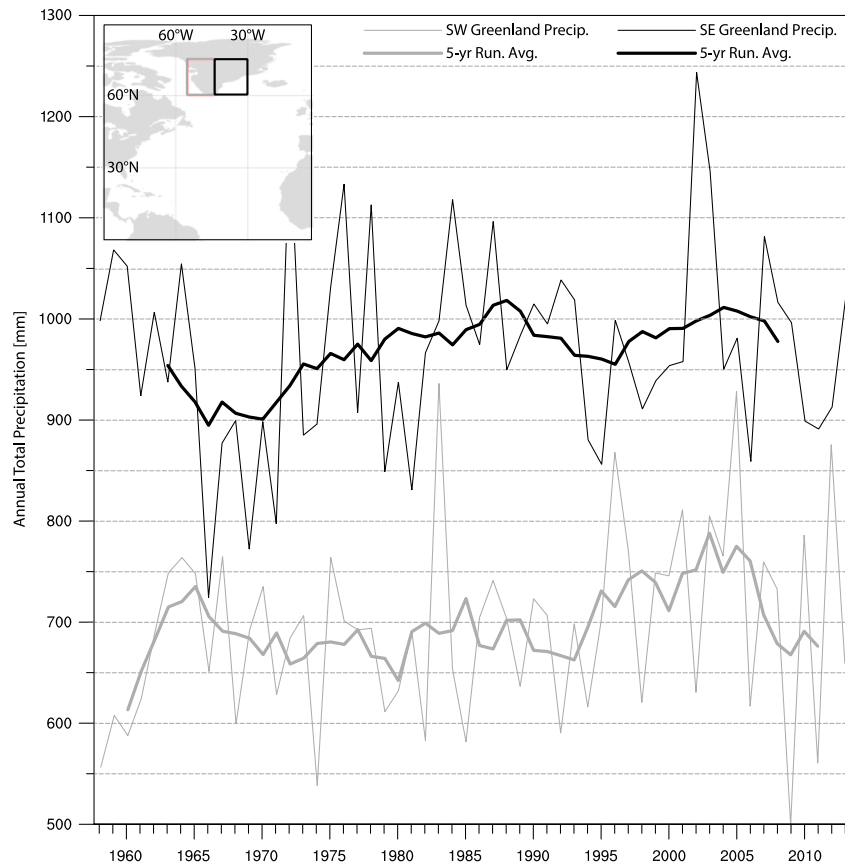
Figure 2. Southwest (gray) and southeast (black) Greenland precipitation output from JRA-55 over 1958–2013.

dominated by northeasterly winds. These wind patterns can be explained by the climatological Greenland High anticyclone.

Figure 2 shows the interannual variability of total annual precipitation in both southwest (gray) and southeast (black) Greenland as modeled by JRA-55. These precipitation signals differ both in interannual variability and in long-term trends ($p < 0.05$). Total annual precipitation and interannual variability of the signal increase during the years 1970 to 2013 in southwest Greenland, whereas southeast Greenland shows an increase in variability during the years 1970 to 1990, with a general decrease in interannual variability to 2000. The total annual precipitation amount is greater in the southeast with respect to the southwest by as much as 2000 mm/yr in some regions (Figure 1e) and more than 200 mm/yr averaged over the whole areas (Figure 2). Southeast Greenland receives more precipitation during the winter (DJF; ~200 mm/yr), spring (MAM; ~75 mm/yr), and autumn (SON; ~55 mm/yr) months, with respect to the southwest, while receiving slightly less precipitation than the southwest during the summer (JJA; ~30 mm/yr) months when *Schuenemann et al.* [2009] found Baffin Bay cyclones to occur more frequently and contribute to orographic lift in southwest Greenland. During the transitional and winter seasons, strong cyclones approaching Greenland from the North Atlantic storm track cause large precipitation events on the southeast coast of Greenland due to moist, cyclonic, upslope flow, contributing to the local maximum in precipitation on the southeast coast [*Schuenemann et al.*, 2009; *Chen et al.*, 1997]. The higher amount of annual precipitation in southeast Greenland is due to the increased number of cyclones that expire in the Icelandic region rather than over the Labrador Sea [*Schuenemann and Cassano*, 2009]. The Icelandic Low (blue center in Figure 1b) is seen in the monthly, seasonal, and annual averages of low MSLP in the North Atlantic, due to the general Icelandic location of the climatological low pressure center. The Icelandic Low is one of two poles that make up the derived climate index, the North Atlantic Oscillation (NAO; Figure 3).

The NAO is defined as the fluctuation in the meridional gradient of the MSLP between Iceland and the Azores Islands. The phenomenon was named by *Walker and Bliss* [1932]; pattern first mentioned by *Walker* [1923]
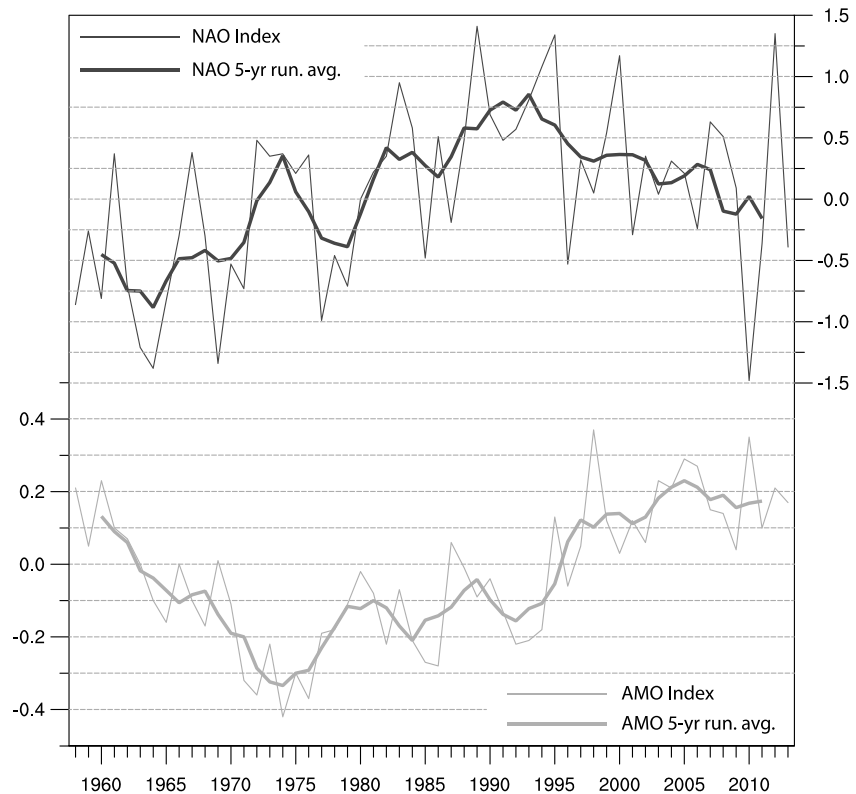
Figure 3. NAO (black) and AMO (gray) indices (thin lines) with their 5 year running means (thick lines) over 1958–2013.

who described the NAO as the tendency of the coordinated strengthening or weakening of the Icelandic Low and the Azores High, which are climatological features seen in monthly, seasonal, and annual MSLP fields over the North Atlantic. A strengthening of the Icelandic Low and Azores High creates a steeper meridional MSLP gradient (+NAO) accompanied by increased near-surface winds, whereas a weakening of these features forms a weaker meridional MSLP gradient (−NAO) accompanied by decreased near-surface winds. *Rogers* [1990] connected the MSLP patterns in the North Atlantic to cyclone tracks and found that during extreme +NAO years, the Icelandic Low was deeper and located east of southern Greenland leading to a strong MSLP gradient, which he linked to the meridional cyclone frequency gradient. Conversely, during extreme −NAO years, the center of highest cyclone frequency (Icelandic Low) was located farther southwest, off the coasts of New England and the Canadian Maritimes. *Serreze et al.* [1997] found that cyclone frequency and intensity more than doubled during +NAO years when compared to −NAO years.

We test another climate index located in the North Atlantic hypothesized to be linked to precipitation in southern Greenland: the Atlantic Multidecadal Oscillation (AMO; Figure 3). The AMO is a well-known climate pattern in the North Atlantic but is not as well understood as the NAO. The AMO index describes the multi-decadal variation of sea surface temperature (SST) in the North Atlantic Basin, a phenomenon first identified by *Schlesinger and Ramankutty* [1994]. *Enfield et al.* [2001] defined the AMO index as the linearly detrended, 10 year running mean of SST anomalies with respect to the 1856–1999 mean using the Extended Reconstructed SST [*Kaplan et al.,* 1998] gridded data set. *Wunsch* [1992] notes that a widespread North Atlantic basin SST oscillation is difficult to claim as driven by internal forces based on the sparse observational data from the oceans. Despite this, the AMO is widely suggested to originate from variations in the Atlantic Meridional Overturning Circulation (AMOC), a phenomenon through which the thermohaline circulation [driven by density gradients due to temperature and salinity; *Delworth and Mann*, 2000] and buoyancy forcing [driven by density differences due to freshwater input; *Otterå et al.,* 2010] are thought to provide the key driving stresses for the northeastward flow of the Gulf Stream. *Wunsch and Ferrari* [2004] clearly described ocean circulation and mixing as controlled by wind. Furthermore, *Wunsch* [2006] argued that in
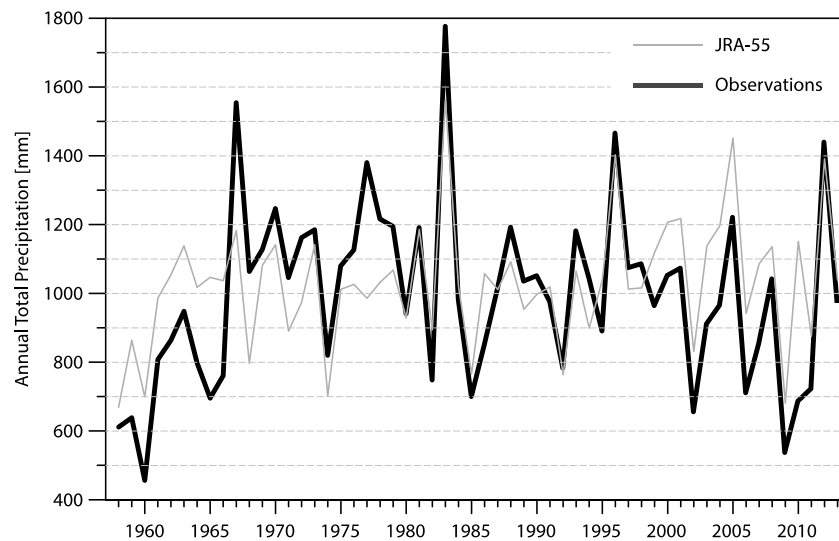
Figure 4. Nuuk, Greenland precipitation observations (black) and JRA-55 precipitation output over Nuuk (gray) in millimeter per year over 1958–2013.

order to solve for the net meridional property flux (equation 2 in manuscript), the variables needed are not resolved in the current climate models. Using an atmospheric general circulation model coupled to a 50 m thick slab-ocean model, *Clement et al.* [2015] found that the simulated North Atlantic SST variations closely resemble those found in the AMO, which suggests that the AMOC is not necessary to explain the AMO index. Similarly, *Birkel and Mayewski* [2015] ascribe the origin of the AMO to wind-stress forcing that develops following major volcanic eruptions. Their claim is deduced from the strong coincidence between measurements of high stratospheric aerosol content and cool SSTs. Birkel and Mayewski show that SSTs in the North Atlantic subpolar region south of Greenland (beneath the westerly wind belt) covary with 10 m wind speeds, as well as the strength of the West African Monsoon, together implying a basin-wide atmospheric link.

2. Data and Methods

2.1. Atmospheric Reanalysis

We begin our analysis of southern Greenland precipitation by first validating the JRA-55 modeled precipitation to observations in Nuuk, Greenland (64.2°N, 51.7°W). Weather observations over Greenland are sparse, and therefore, efforts here are primarily dependent on utilizing output from gridded climate reanalyses. Of the several available reanalysis models, we use JRA-55 because it provides the longest record of all available third generation reanalyses (NCEP/NCAR CFSR, ECMWF ERA-Interim, and NASA MERRA all start in 1979, whereas JRA-55 begins in 1958) and also proves to reliably reproduce monthly and annual total precipitation with respect to observations at Nuuk, as demonstrated later in this paper. When first released, JRA-55 spanned the years 1958 (following the International Geophysical Year, beginning of continuous global radiosonde observations) to 2012. At the time of this analysis, JRA-55 has been extended to 2013. Monthly output for JRA-55 was obtained from the NCAR Computational Information Systems Laboratory (CISL) Research Data Archive (RDA; http://rda.ucar.edu) under ds628.1, as found on the Yellowstone supercomputer.

2.2. Nuuk Observations

Weather station records in southern Greenland commonly span only 5–10 years. Observations from Nuuk, however, contain a near-continuous record of precipitation spanning 1958 to present with only 151 days of missing precipitation data out of the total 20,454 days, or 0.7% of the record. Of the 151 missing days, 69 are missing from 01 January to 30 April 2013, whereas the remaining 82 missing days are spread evenly across the remainder of the data record, with less than 3 days missing in a given month. Other long precipitation records in southern Greenland contain large gaps on the order of 20–40% of missing daily precipitation observations. The daily Nuuk precipitation observations are obtained from the Global Historical Climatology
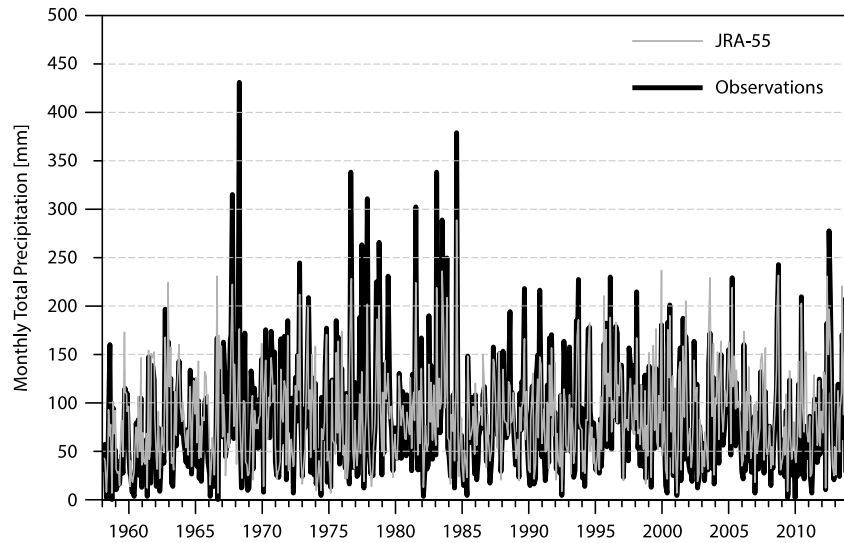
Figure 5. Nuuk, Greenland precipitation observations (black) and JRA-55 precipitation output over Nuuk (gray) in millimeter per month over 1958–2013.

Network (GHCN) at NOAA National Centers for Environmental Information (NCEI). For this paper, the daily precipitation amounts are summed into annual (Figure 4) and monthly (Figure 5) totals.

2.3. Reanalysis Validation

The JRA-55 precipitation was validated by correlating to Nuuk observations. As we are comparing a point observation to gridded model output, the comparison is better suited for temporal averages [*Ensor and Robeson*, 2008], annual and monthly totals. Annual totals compare well against JRA-55 output ($r = 0.72$). As seen in Figure 4, the correlation preceding 1979 is much lower than that of the years following 1979 ($r = 0.60$ and 0.81, respectively). Thus, the integration of satellite data from 1979 onward has, as expected, added significant confidence with respect to the interpretation of precipitation in JRA-55, at least over this location. Monthly precipitation (Figure 5) totals correlate very well with JRA-55 output over Nuuk ($r = 0.86$), but unlike the annual totals, the correlation coefficient does not increase as substantially from before to after 1979 ($r = 0.84$ and 0.89, respectively).

Less precipitation falls during winter and early spring months with an increase of precipitation during late summer and fall months. The decreased precipitation during winter months is partly due to the Greenland High, as mentioned earlier, which blocks low pressure centers (storms) from traversing much of Greenland. The Greenland High is most prominent during winter months due to extreme katabatic flow (i.e., continuous cold, dense air flowing from high to low elevations) from a lack of local incoming solar radiation. As JRA-55 also captures seasonality seen in the observations, the monthly correlation coefficient is improved over the annual correlation.

Table 1 shows that the 56 year total precipitation difference between Nuuk observations and JRA-55 output is about −2000 mm. The JRA-55 precipitation output is higher than that of the observed precipitation, an average difference of 36 mm/yr or 3 mm/month.

2.4. Indices

The NAO (Figure 3) reflects the climatological pressure difference between the Icelandic Low and Azores High, which can be seen in the leading empirical orthogonal function (EOF) of the northern hemisphere

Table 1. Nuuk Precipitation Differences From Observations Subtract JRA-55 Output for Monthly and Annual Totals[a]

	Mean Difference	Mode (Times)	Standard Deviation	Total Diff.
Monthly	−3	−14 (21)	30	−2013
Yearly	−36	−152 (2)	177	−2002

[a]The standard deviation is of the difference. All monthly and annual totals are rounded to nearest millimeter.
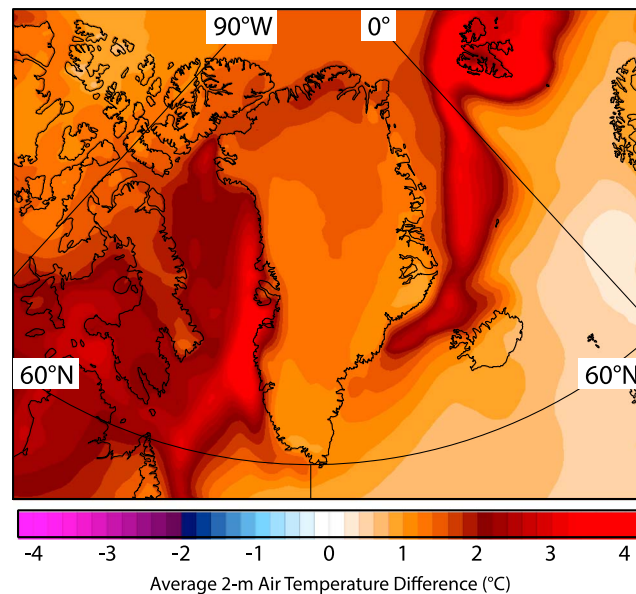
Figure 6. The 2 m temperature difference with respect to the AMO phases, +AMO (1996–2013) subtract −AMO (1964–1994) (°C).

MSLP anomalies, explaining 42.8% of the DJFM variance [*Hurrell et al.*, 2003]. Although the NAO describes the winter MSLP gradient, the gradient does exist, albeit more subdued, during the rest of the year and can be seen in the leading EOF of MSLP through the other seasons (MAM, JJA, and SON). The variance explained by the first EOF decreases through the seasons (MAM, 33.6%; JJA, 27.9%; and SON, 22.6%) with the annual anomaly variance explained at 32.4% [*Hurrell et al.*, 2003]. This EOF-based NAO index and EOF information can be found at the NCAR UCAR Climate Data Guide website (https://climatedataguide.ucar.edu/climate-data/hurrell-north-atlantic-oscillation-nao-index-pc-based).

The AMO index used here (Figure 3) is derived using a similar method to that of *Enfield et al.* [2001] with a few changes. The annual North Atlantic SST anomalies shown in Figure 3 are based on the 20th century average, rather than the 1864–1999 average as in *Enfield et al.* [2001], and not detrended, thus preserving the long-term warming trend. Linearly detrending, the SST anomaly signal emphasizes the multidecadal characteristics but removes the underlying warming trend caused by anthropogenic factors. The detrended AMO index is not suitable for this study because the recent anthropogenic warming is part of the southern Greenland precipitation investigation. The AMO index used here not only shows the multidecadal fluctuations of the North Atlantic SST over the last seven decades but also displays the overall increasing SST coinciding with the enhanced warming in the Arctic [*Serreze and Francis*, 2006]. The JRA-55 reanalysis encompasses one −AMO and one +AMO phase. The year 1963 marks the beginning of the recent AMO "cycle" resulting in a full −AMO phase (1964–1994) of anomalously cooler North Atlantic annual SSTs and the current +AMO phase (1996–2013) of anomalously warmer annual SSTs.
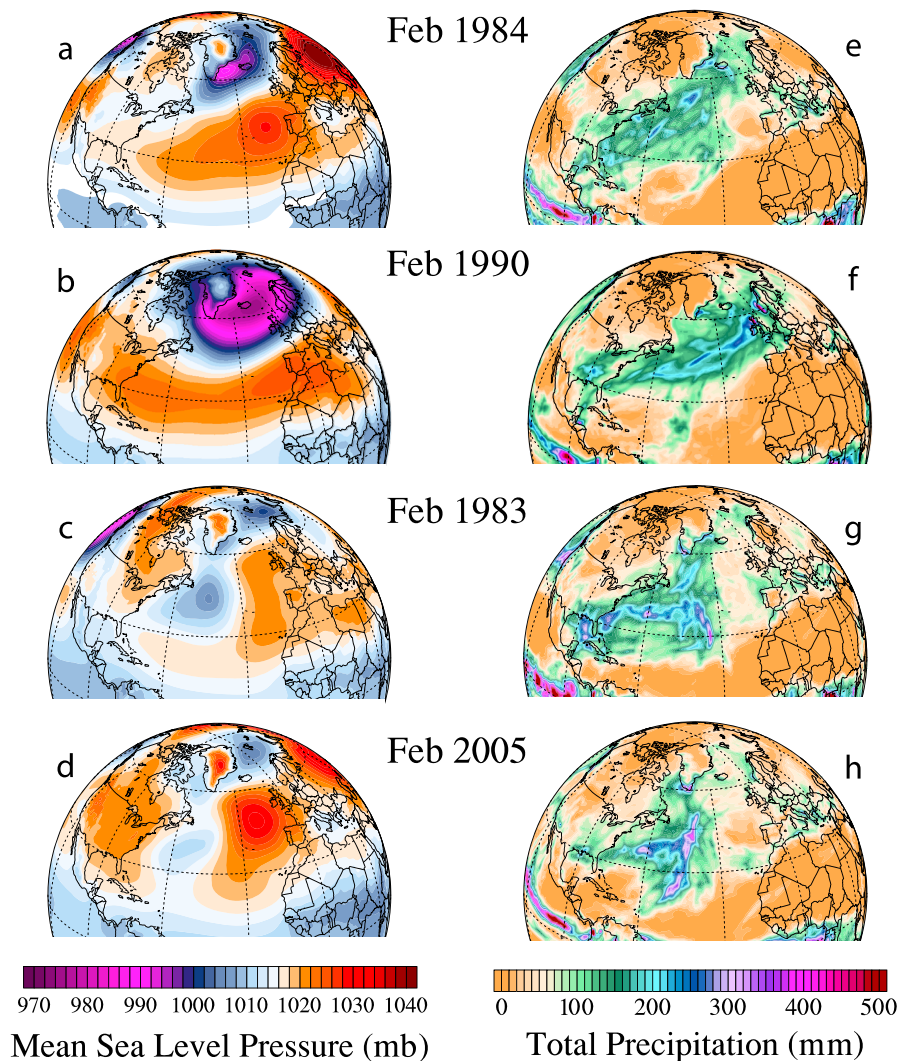
While the NAO and AMO indices are useful for identifying changes in general circulation since they combine several aspects of atmospheric states, the indices alone do not explain the driving forces of synoptic weather. In the case of the NAO, cyclone frequency [*Rogers*, 1990; *Serreze et al.,* 1997] and near-surface westerlies [*Rogers*, 1985] are the major drivers of T_{2m} and precipitation over the coastal regions of the North Atlantic domain, which in many cases correlate well with the NAO index. For the same reasons, we look to near-surface wind patterns driving the AMO. We favor the argument that North Atlantic SST is externally driven by the westerlies, as explained by *Wunsch and Ferrari* [2004]. Changes in wind stress stimulate ocean surface mixing and SST, and changes in atmospheric circulation lead to altered spatial signatures of T_{2m} and precipitation. Thus, it is expected that T_{2m} and precipitation measured proximal to the North Atlantic correlate well with the AMO index.

2.5. The Icelandic Low and the Azores High

In our search to explain changes in southern Greenland precipitation, we examine both of the pressure centers that define the NAO, the Icelandic Low and Azores High, and their association with the basic climatological variables T_{2m}, u_{10m}, v_{10m}, and precipitation. We first identify the locations of the seasonal and annual Icelandic Low and Azores High to show how both climatological pressure centers fluctuate and to correlate them to precipitation in southern Greenland. There are two options, namely, the average of a stationary or of a floating location. The Icelandic Low location is conventionally found within the Denmark Strait/Iceland region. However, the Icelandic Low is not stationary, and it can be found in other locations, such as south of Greenland or farther north over the Greenland and Norwegian seas. Here we focus on the Icelandic Low

Figure 7. (left) Mean sea level pressure and (right) precipitation averaged over February months of extreme precipitation and NAO phases. (a and b) Positive NAO examples with (e and f) decrease in southwest Greenland precipitation. (c and d) Negative NAO examples with (g and h) increase in southwest Greenland precipitation.

in the most common location (proximal to Iceland) rather than the Icelandic Low changing locations through time. Going with the first option is important for this investigation because of the counterclockwise flow around cyclones and these winds in the vicinity of southern Greenland. Thus, we define the Icelandic Low as the average of monthly and yearly MSLP within 58°N–68°N and 20°W–40°W as per the first option.

The same approach is taken for defining the Azores High. Although the Azores High is generally more stationary when compared to the Icelandic Low, the general high pressure center locations fall over the Azores Islands or southwestern Europe (France and the Iberian Peninsula). Here we define the Azores High as the monthly and annual MSLP averaged over 20°N–40°N and 20°W–40°W. We also show that, however rare, high pressure blocking patterns can persist over the northeast Atlantic from a few days to a couple of weeks. The blocking events local to the Azores Islands, as described here, differ from Greenland blocking. Greenland blocking is formed by the Greenland high, most prominent during winter months, and persists, though can increase and decrease in strength, throughout the year.

3. Results

As discussed above, southern Greenland is climatologically divided into two areas, the southwest and southeast. The evolution of precipitation in southwest and southeast Greenland will be discussed. Then, the
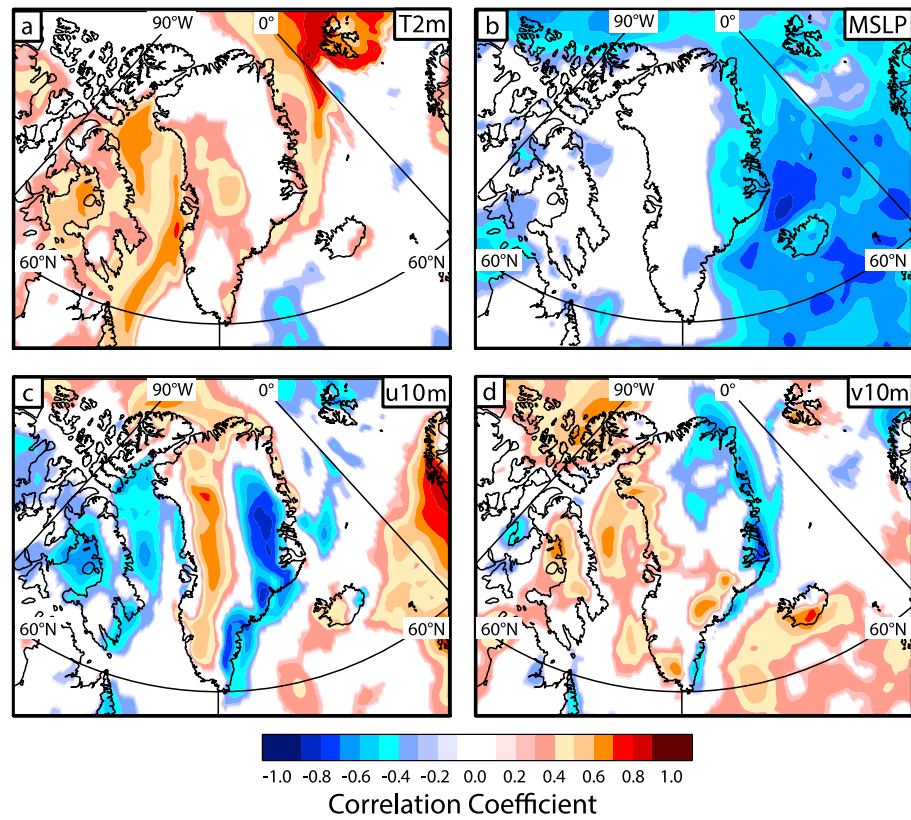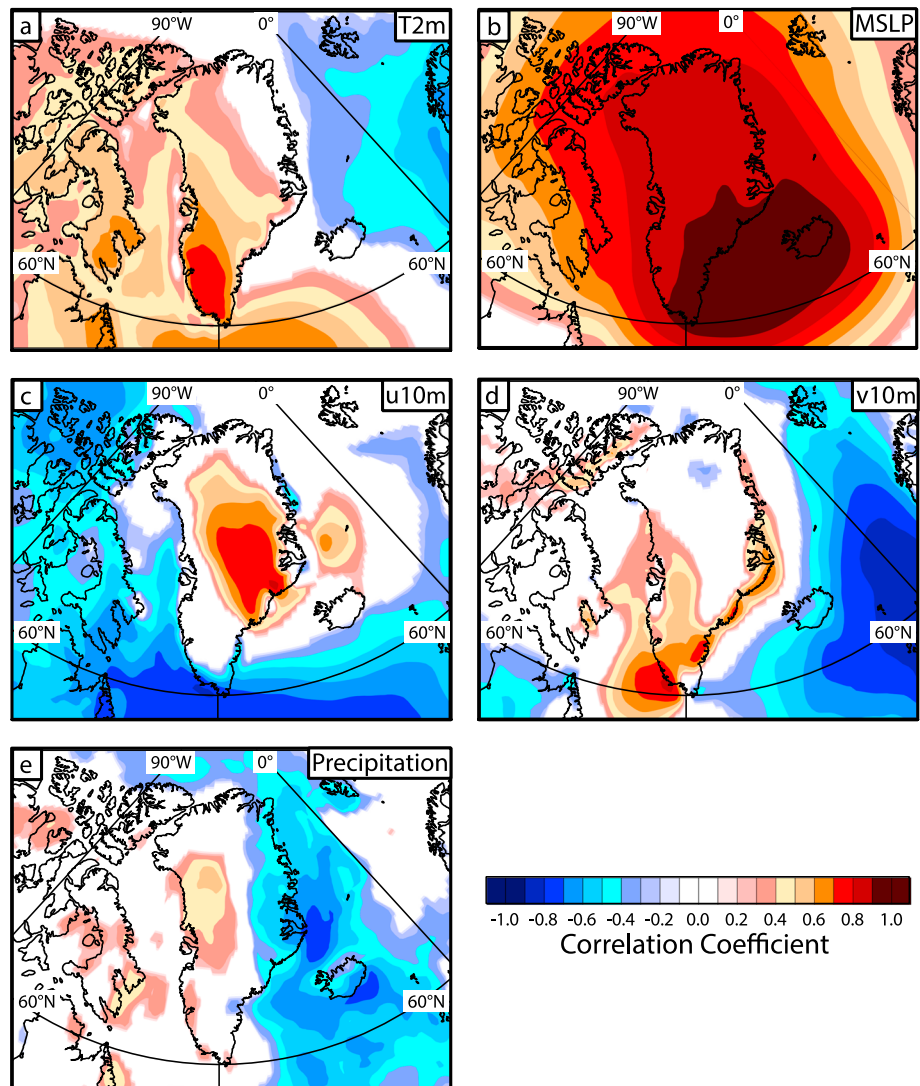
Figure 8. Annual correlation maps between precipitation and (a) 2 m temperature (T_{2m}), (b) mean sea level pressure (MSLP), (c) 10 m u winds (u_{10m}), and (d) 10 m v winds (v_{10m}) over 1958–2013. All contours are within the 95% confidence level.

interannual variability of precipitation in both regions is presented with respect to how the Icelandic Low, Azores High, T_{2m}, 10 m winds, and blocking patterns influence precipitation across southern Greenland.

The mean annual total precipitation over southwest Greenland (as shown by the gray box in Figure 2) is 723 mm/yr. Precipitation between 1964 and 1994 is generally lower than the mean, at an average of 693 mm/yr, whereas after 1995, precipitation increases by about 9%, to an average of 753 mm/yr (Figure 2). The standard deviation of southwest Greenland precipitation also increases, by about 61%, from 66 to 106 mm/yr ($p < 0.05$). The increase in precipitation and interannual variability corresponds to the shift from the −AMO to +AMO phase in 1995 (Figure 3). Additionally, this increase parallels the general increase in T_{2m} over southern Greenland (Figure 6), which also corresponds to the 1995 AMO shift. Furthermore, the increase in SSTs since 1995 coincides with the recent enhanced warming of the Arctic (section 2.4).

The mean annual total precipitation in southeast Greenland (as shown by the black box in Figure 2) is 970 mm/yr and shows a different pattern when compared to southwest Greenland precipitation. During the 1958–1983 period, southeast Greenland precipitation appears to be more variable than during the 1984–2001 period, with an apparent increase in variability following 2001. However, the described time periods fail the student t test ($p \gg 0.05$), suggesting that precipitation in southeast Greenland has not fluctuated on any long-term basis, at least as produced by JRA-55.

The interannual extremes of both southwest and southeast Greenland precipitation coincide with the temporal changes of the strength of the Icelandic Low (supporting information Figure S1); when the Icelandic Low is deep (weak), southeast (southwest) Greenland receives an increase in precipitation. One would therefore expect an anticorrelation between precipitation in southwest and southeast Greenland, but this is not the case ($r = 0.06$). As low pressure systems traverse the North Atlantic from the northeastern United States to Iceland, the Icelandic Low is found to be deep and situated proximal to Iceland [*Rogers*, 1990], as can be seen in examples from February 1984 and 1990 (Figure 7). Conversely, as cyclones take a

Figure 9. Annual correlation maps between the Icelandic Low and (a) 2 m temperature (T_{2m}), (b) mean sea level pressure (MSLP), (c) 10 m u winds (u_{10m}), (d) and 10 m v winds (v_{10m}) over 1958–2013. All contours are within the 95% confidence level.

more variable path, the Icelandic Low is generally weaker and can be found south of Greenland. This can be explained by a decrease in westerly wind speeds [*Rogers*, 1985], a decrease in frequency of low pressure systems [*Rogers*, 1990; *Serreze et al.*, 1997], and/or high pressure blocking patterns over the northeast Atlantic [*Barnston and Livezey*, 1987; *Corte-Real et al.*, 1998]. Examples of the latter are seen during the Februarys of 1983 and 2005 (Figures 7c, 7d, 7g, and 7h).

Precipitation in the topographically divided region of southern Greenland correlates to u_{10m} (Figure 8c, and Figure S2 for seasonal correlations) on either side of the ridgeline, positively ($0.5 < r < 0.7$, $p < 0.05$) to the west and negatively ($-0.7 < r < -0.5$, $p < 0.05$) to the east, as expected, since orographic flow increases chances for precipitation. The easterlies, which influence precipitation in southeast Greenland, can occur with cyclonic flow in the Denmark Strait (Figure S1), thus seasons when the Icelandic Low is deep, such as DJF and MAM. On the other side of Greenland, precipitation chances are expected to increase in the southwest when the Icelandic Low is weak, as demonstrated by the winter and spring correlations of 0.5–0.7 ($p < 0.05$) between the Icelandic Low and precipitation (Figure S1). This weak Icelandic Low pattern is associated with increasing meridional winds over southwest Greenland as seen in the correlations between the Icelandic Low and v_{10m} (0.5–0.7, $p < 0.05$; Figure 9d). As the Icelandic Low is more
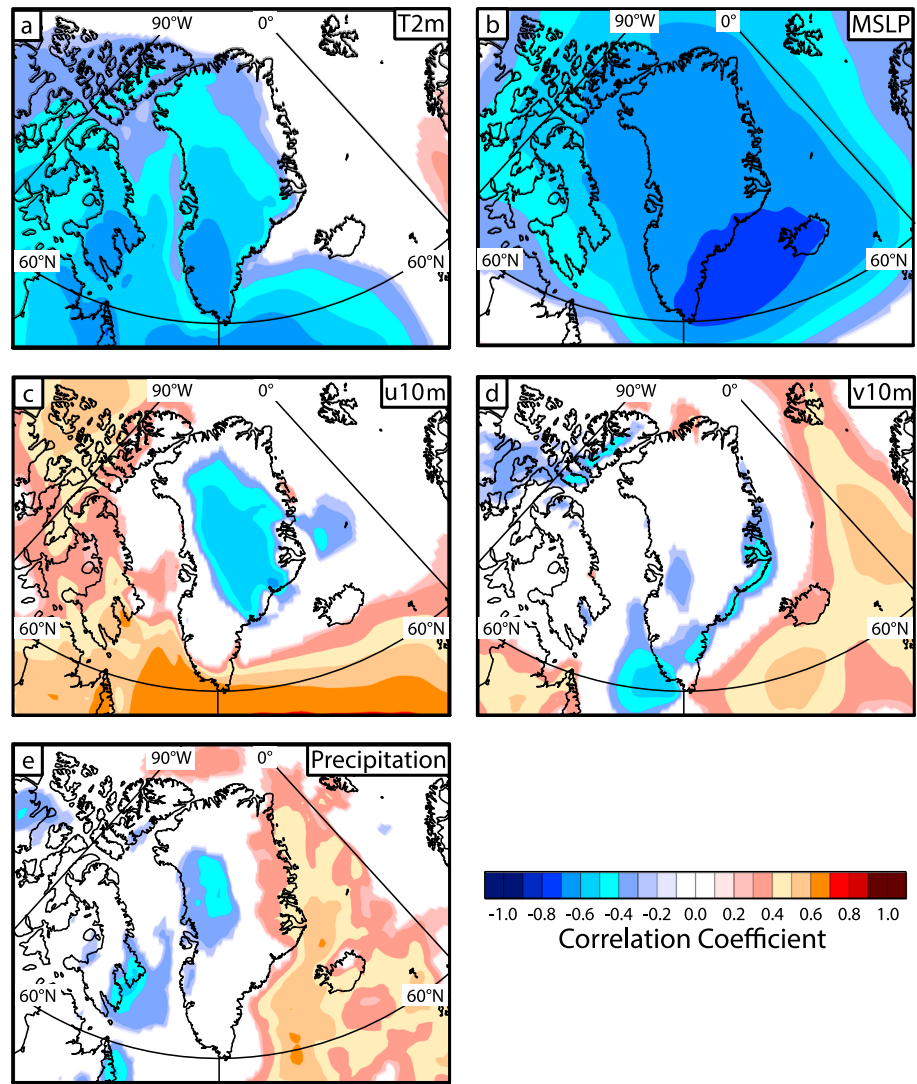
Figure 10. Annual correlation maps between the Azores High and (a) 2 m temperature (T_{2m}), (b) mean sea level pressure (MSLP), (c) 10 m u winds (u_{10m}), and (d) 10 m v winds (v_{10m}) over 1958–2013. All contours are within the 95% confidence level.

pronounced in winter months, and to a lesser extent the spring, the correlations between the Icelandic Low and precipitation and v_{10m} correlations decrease through summer and autumn ($0.4 < r < 0.6$, $p < 0.05$) in southwest Greenland (Figure S3).

Blocking patterns over the northeast Atlantic also play a role in where precipitation may fall over southern Greenland. With persistent, high pressure blocking patterns over the northeast Atlantic, low pressure systems will take a poleward path around the high due to the outward, clockwise (anticyclonic) flow around the high. These blocking patterns can appear in the climatological Azores High, as seen in the Februarys of 1983 and 2005. As discussed earlier, it should be noted that blocking patterns are rare. The Azores High has a lower correlation ($-0.4 < r < 0.0$, $p < 0.05$) with precipitation, u_{10m}, and v_{10m} than the Icelandic Low has (Figure 10 compared to Figure 9). However, lower T_{2m} in southern Greenland correlate ($-0.7 < r < -0.6$, $p < 0.05$) with a stronger Azores High (Figure 10a), and higher surface temperatures correlate with a stronger Icelandic Low (Figure 9a), as expected. The correlations between the Azores High and precipitation in southern Greenland are nonexistent ($-0.1 < r < 0.1$; Figure 10e) showing that the Azores High plays little to no role in the interannual variability of southern Greenland precipitation. Therefore, this result should suggest caution when using the NAO index, which combines
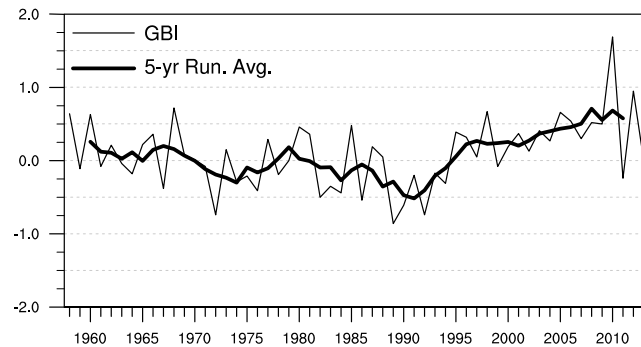
Figure 11. Greenland Blocking Index (GBI; thin line) with the 5 year running mean (thick line) over 1958–2013.

the Icelandic Low and the Azores High, to explain fluctuations of precipitation in southern Greenland, and perhaps other regions.

However, high pressure blocking patterns in the Azores Islands region are shown to play a large role during 2 years of extreme high precipitation in southwest Greenland, 1983 and 2005. February of both years (Figures 7c and 7d) shows not only a weak Icelandic Low located south of Greenland but also a strong Azores High extending northward when a block persisted for close to two weeks. This led to a northward cyclone path toward southern Greenland. In these cases, southwest Greenland received more precipitation than other years, while the southeast received less.

4. Discussion

The existence of blocking patterns influences cyclone tracks, thus increasing precipitation chances over southwest Greenland. The hypothesis put forth by *Francis and Vavrus* [2012] suggests that these blocking patterns will increase in frequency and intensity. During the 1990s and 2000s, the Arctic near-surface temperature increased at nearly twice the rate of the northern hemisphere [*Serreze et al.,* 2009; *Screen and Simmonds*, 2010]. This enhanced warming, or Arctic amplification, was caused by the increase in greenhouse gases and positive feedback loops regarding sea ice, high latitude snow cover, water vapor, and cloud cover [*Stroeve et al.,* 2012]. *Francis and Vavrus* [2012] found that Arctic amplification facilitated slower progression of Rossby waves leading to more persistent, long-amplitude waves, which had increased in frequency since 2000. However, *Screen and Simmonds* [2013] showed through Fourier decomposition that links found between Arctic amplification and midlatitude atmospheric circulation are limited to the summer (JAS), and to a lesser extent the autumn (OND), months. They also show that the meridional anomalies are constrained over Europe and zonal anomalies over Asia, in contrast to the *Francis and Vavrus* [2012] study area of North America and North Atlantic. *Barnes* [2013] used least squares regression on 500 mb heights, *v* winds at 250 mb, and *u* winds at 500 mb and showed that a slowing of the westerly winds was significant only in autumn (OND) over the 1980–2011 period. *Barnes* [2013] also indicated that there was no significant increase of blocking events in any season using their methods. *Hopsch et al.* [2012] acknowledged that the *Francis and Vavrus* [2012] results are reasonable but concluded that the observational record is too scarce to confirm their findings. Furthermore, *Walsh* [2014] discussed the difficulties of linking Arctic amplification to mid-latitude weather through the interannual variability signal. *Walsh* [2014] concluded that the midlatitudes will inevitably be affected by the enhanced warming of the Arctic and increased sea ice loss; however, over short time periods, such as the observational record within the Arctic thus far, the climate signal due to greenhouse warming is not long enough to emerge over the "noise" of interannual variability within the Arctic.

Francis and Vavrus [2015] responded and applied new methods on the 1000–500 mb thickness and 500 mb heights, again concluding that the jet stream has become "wavier" since 1995. They offered a new index to characterize waviness of wind flow, the Meridional Circulation Index. Using this new metric, they found that Arctic amplification indeed influenced the zonal wind speed of the flow aloft, thus allowing it to become wavier. They also found that, no matter the season, when the meridional thermal gradient weakens, the *u* winds decrease and the *v* winds increase, again leading to increased waviness and meridional transport.

The increased waviness of atmospheric Rossby waves can be seen in the Greenland Blocking Index [GBI; *Fang*, 2004; *Hanna et al.,* 2016]. The GBI is a simple index explaining the geopotential height at the 500 mb pressure level over Greenland (60–80°N, 20–80°W). Figure 11 shows the standardized version from that of *Hanna et al.* [2016] during the period overlapping the JRA-55 record, 1958–2013. Since the early 1990s, the 10 year running mean of the GBI has been steadily increasing, showing that Greenland blocking events are becoming more frequent. They also show that the GBI mean increased significantly during summer months, as well

as an increase in variability in December months. The interannual variability in GBI values has also increased over the past few years, lining up with findings here on southwestern Greenland precipitation variability. Furthermore, *Hanna et al.* [2016] show that extreme GBI events clearly change the jet stream shape in both the upstream and downstream directions, implying that this has major implications for midlatitude weather. Lastly, they demonstrate that anomalies between the 10 highest and 10 lowest GBI years for DJF precipitation in southern Greenland are greater than 60 mm/season, meaning that more warm, moist air is advected to these latitudes during extreme high GBI years.

Francis and Vavrus [2012, 2015] hypothesized an increase in the meridional transport, which also was shown by *Hanna et al.* [2016]. If Februarys 1983 and 2005 (Figures 7c, 7d, 7g, and 7h) are idealized cases of this scenario, enhanced southwest Greenland precipitation and variability may result. *Schuenemann and Cassano* [2010] found an approximate 20% increase in southern Greenland precipitation projected by 2081–2100 in a middle of the road emissions scenario (A1B from three top-performing CMIP4 models) as compared to ERA-40 precipitation from 1961 to 1999. While much of this projected increase in precipitation was determined through a self-organizing map technique, resulting from increased moisture due to future increased temperatures, the Greenland precipitation changes due to weather pattern changes indicated a strong increase of precipitation in southwest Greenland and a strong decrease in southeast Greenland. Although the reasons for the projected weather pattern change may or may not be due to increased waviness, the weather patterns projected to increase in frequency in *Schuenemann and Cassano* [2010] do appear to be those one might associate with the same high pressure blocking pattern in Figures 7c and 7d, which has led to the same resulting increase in southwestern Greenland precipitation.

5. Summary

This work shows that precipitation, T_{2m}, and 10 m horizontal winds over southern Greenland coincide most closely with the controllers of the NAO and AMO and less so with the indices themselves. However, it should be noted that both the NAO and AMO begin as a negative phase and end in a positive phase during the JRA-55 record, which coincides with the enhanced increase of Arctic T_{2m} and weakening of the meridional thermal gradient. As discussed earlier, an increase in meridional advection, south to north, facilitates the increase in temperature at high latitudes leading to an increase in moisture availability. Not only are these circulation features part of the positive feedback system associated with Arctic amplification, as hypothesized by *Francis and Vavrus* [2015], but these features also increase chances for precipitation in southwest Greenland over a long-term basis. A decrease in the near-surface zonal winds, due to a weakening meridional thermal gradient, facilitates an increase in SST, by reducing sea surface mixing. The recent increase in North Atlantic SST is manifested in the positive mode of the AMO. Furthermore, as the meridional component of the wind field increases due to elongated, slow-moving ridges, precipitation and temperature across southern Greenland will increase, due to increased southerly advection of moisture and heat.

For the 2 years of extreme high precipitation (1983 and 2005; Figure 7), the February 1983 Icelandic Low is located south of Greenland with a high pressure blocking pattern persisting to the east for 2 weeks. In February 2005, the Icelandic Low is almost nonexistent in association with another strong blocking pattern, again just west of Europe. As these blocking patterns develop, cyclones travel poleward west of the high pressure center and, in these cases, to southwest Greenland. In the absence of a blocking pattern, as seen in February of 1984 and 1990 (Figure 7), cyclones take a predominantly northeastward path toward Iceland and Great Britain [*Hurrell*, 1995] bringing more precipitation to southeast Greenland and less to southwest Greenland. The seasonal correlations between the Icelandic Low and precipitation are strongest during the winter, when the low pressure system is most prominent (Figure S1).

In conclusion, precipitation across southern Greenland is part of a complex system partially explained by the Icelandic Low, T_{2m}, u_{10m}, v_{10m}, and blocking patterns. The strength of the Icelandic Low appears to be one of the major controllers of southern Greenland precipitation (Figures 9 and S1) operating in tandem with increasing T_{2m} (Figure 6), southwesterly near-surface wind field over southwest Greenland and southeasterly near-surface wind field over southeast Greenland (Figures S2 and S4). As meridional and zonal wind components increase in the positive direction (southerly and westerly, respectively), the chances for precipitation over southwest Greenland increase, whereas zonal flow increasing in the negative direction (easterly) increases chances for precipitation in southeast Greenland. Southerly flow over the North Atlantic is often

accompanied with an increase in temperature and moisture, thus increasing chances for precipitation across southern Greenland. It should be expected that if enhanced Arctic warming increases through time, elongated ridging and blocking patterns should increase in frequency [*Hanna et al.,* 2016], thus increasing precipitation over southwest Greenland, both in annual amount and variability, while decreasing the likelihood of precipitation over southeast Greenland. However, it should be noted that the long-term trend in southeast Greenland precipitation is unchanging over the JRA-55 record, therein showing the complexity of linkages between blocking patterns and climate in southeast Greenland.

References

Barnes, E. A. (2013), Revisiting the evidence linking Arctic amplification to extreme weather in midlatitudes, *Geophys. Res. Lett.*, *40*, 4734–4739, doi:10.1002/grl.50880.

Barnston, A. G., and R. E. Livezey (1987), Classification, seasonality and persistence of low-frequency atmospheric circulation patterns, *Mon. Weather Rev.*, *115*, 1083–1126.

Birkel, S. D., and P. A. Mayewski (2015), Analysis of historical and projected future climate of Mali, West African Sahel, Project Report. CGIAR Research Program on Climate Change, Agriculture and Food Security (CCAFS), Copenhagen. [Available at http://www.ccafs.cgiar.org.]

Chen, Q.-S., D. H. Bromwich, and L. Bai (1997), Precipitation over Greenland retrieved by a dynamic method and its relation to cyclonic activity, *J. Clim.*, *10*, 839–870.

Clement, A., K. Bellomo, L. N. Murphy, M. A. Cane, T. Mauritsen, G. Rädel, and B. Stevens (2015), The Atlantic Multidecadal Oscillation without a role for ocean circulation, *Science*, *350*, 320–324.

Corte-Real, J., B. Qian, and H. Xu (1998), Regional climate change in Portugal: Precipitation variability associated with large-scale atmospheric circulation, *J. Clim.*, *18*, 619–635.

Delworth, T. L., and M. E. Mann (2000), Observed and simulated multidecadal variability in the Northern Hemisphere, *Clim. Dyn.*, *16*, 661–676.

Doyle, J. D., M. A. Shapiro, Q. Jiang, and D. L. Bartels (2005), Large-amplitude mountain wave breaking over Greenland, *J. Atmos. Sci.*, *62*, 3106–3126.

Enfield, D. B., A. M. Mestas-Nuñez, and P. J. Trimble (2001), The Atlantic multidecadal oscillation and its relation to rainfall and river flows in the continental U.S, *Geophys. Res. Lett.*, *28*, 2077–2080, doi:10.1029/2000GL012745.

Ensor, L. A., and S. M. Robeson (2008), Statistical charicteristics of daily precipitation: Comparisons of gridded and point datasets, *J. Appl. Meteorol. Climatol.*, *47*, 2468–2476.

Fang, Z.-F. (2004), Statistical relationship between the northern hemisphere sea ice and atmospheric circulation during winter time, in *Observation, Theory and Modeling of Atmospheric Variability*, World Sci. Ser. Meteorol. East Asia, edited by X. Zhu, pp. 131–141, World Sci., Singapore.

Francis, J. A., and S. J. Vavrus (2012), Evidence linking Arctic amplification to extreme weather in mid-latitudes, *Geophys. Res. Lett.*, *39*, L06801, doi:10.1029/2012GL051000.

Francis, J. A., and S. J. Vavrus (2015), Evidence for a wavier jet stream in response to rapid Arctic warming, *Environ. Res. Lett.*, *10*.

Hanna, E., T. E. Cropper, R. J. Hall, and J. Cappelen (2016), Greenland Blocking Index 1851–2015: A regional climate change signal, *Int. J. Climatol.*, *36*, 4847–4861.

Hopsch, S., J. Cohen, and K. Dethloff (2012), Analysis of a link between fall Arctic sea ice concentration and atmospheric patterns in the following winter, *Tellus, Ser. A*, *64*, 18,624.

Hurrell, J. W. (1995), Decadal trends in the North Atlantic Oscillation: Regional temperatures and precipitation, *Science*, *269*, 676–679.

Hurrell, J. W., Y. Kushnir, G. Ottersen, and M. Visbeck (2003), *The North Atlantic Oscillation: Climate Significance and Environmental Impact*, Geophys. Monogr. Ser., vol. 134, 279 pp., AGU, Washington, D. C.

Kaplan, A., M. A. Cane, Y. Kushnir, A. C. Clement, M. B. Blumenthal, and B. Rajagopalan (1998), Analyses of global sea surface temperature 1856–1991, *J. Geophys. Res.*, *103*, 18,567–18,589, doi:10.1029/97JC01736.

Kobayashi, S., et al. (2015), The JRA-55 Reanalysis: General specification and basic characteristics, *J. Meteorol. Soc. Jpn.*, *93*, 5–48.

Ohmura, A., and N. Reeh (1991), New precipitation and accumulation maps for Greenland, *J. Glaciol.*, *37*, 140–148.

Otterå, O. H., M. Bentsen, H. Drange, and L. Suo (2010), External forcing as a metronome for multidecadal variability, *Nat. Geosci.*, *3*, 688–694.

Rogers, J. C. (1985), Atmospheric circulation changes associated with the warming over the Northern North Atlantic in the 1920s, *J. Clim. Appl. Meteorol.*, *24*, 1303–1310.

Rogers, J. C. (1990), Patterns of low-frequency monthly sea level pressure variability (1899–1986) and associated wave cyclone frequencies, *J. Clim.*, *3*, 1364–1379.

Schlesinger, M. E., and N. Ramankutty (1994), An oscillation in the global climate system of period 65–70 years, *Nature*, *367*, 723–726.

Schuenemann, K. C., and J. J. Cassano (2009), Changes in synoptic weather patterns and Greenland precipitation in the 20th and 21st centuries: 1. Evaluation of late 20th century simulations from IPCC models, *J. Geophys. Res.*, *114*, D20113, doi:10.1029/2009JD011705.

Schuenemann, K. C., and J. J. Cassano (2010), Changes in synoptic weather patterns and Greenland precipitation in the 20th and 21st centuries: 2. Analysis of 21st century atmospheric changes using self-organizing maps, *J. Geophys. Res.*, *115*, D05108, doi:10.1029/2009JD011706.

Schuenemann, K. C., J. J. Cassano, and J. Finnis (2009), Synoptic forcing of precipitation over Greenland: Climatology for 1961–99, *J. Hydrometeorol.*, *10*, 60–78.

Screen, J. A., and I. Simmonds (2010), The central role of diminishing sea ice in recent Arctic temperature amplification, *Nature*, *464*, 1334–1337.

Screen, J. A., and I. Simmonds (2013), Exploring links between Arctic amplification and mid-latitude weather, *Geophys. Res. Lett.*, *40*, 959–964, doi:10.1002/grl.50174.

Serreze, M. C., and J. A. Francis (2006), The Arctic amplification debate, *Clim. Change*, *76*, 241–264.

Serreze, M. C., F. Carse, and R. G. Barry (1997), Icelandic low cyclone activity: Climatological features, linkages with the NAO, and relationships with recent changes in the Northern Hemispheric circulation, *J. Clim.*, *10*, 453–464.

Serreze, M. C., A. P. Barrett, J. C. Stroeve, D. N. Kindig, and M. M. Holland (2009), The emergence of surface-based Arctic amplification, *Cryosphere*, *3*, 11–19.

Stroeve, J. C., M. C. Serreze, M. M. Holland, J. E. Kay, J. Maslanik, and A. P. Barrett (2012), The Arctic's rapidly shrinking sea ice cover: A research synthesis, *Clim. Change*, *110*, 1005–1027.

Tedesco, M., et al. (2015), Greenland ice sheet. In Arctic Report Card: Update for 2015. [Available at http://www.arctic.noaa.gov/reportcard/greenland_ice_sheet.html.]

Walker, G. T. (1923), Correlation in seasonal variations of weather, VIII: A preliminary study of world weather, *Mem. Ind. Meteorol. Dept.*, *24*, 275–332.

Walker, G. T., and E. W. Bliss (1932), World weather, *V. Mem. R. Meteorol. Soc.*, *103*, 29–64.

Walsh, J. E. (2014), Intensified warming of the Arctic: Causes and impacts on middle latitudes, *Global Planet. Change*, *117*, 52–63.

Wunsch, C. (1992), Decade-to-century changes in the ocean circulation, *Oceanography*, *5*, 99–106.

Wunsch, C. (2006), Abrupt climate change: An alternative view, *Quat. Res.*, *65*, 191–203.

Wunsch, C., and R. Ferrari (2004), Vertical mixing, energy, and the general circulation of the oceans, *Annu. Rev. Fluid Mech.*, *36*, 281–314.